ACTA METALLURGICA SLOVACA
2022, VOL. 28, NO. 3, 157-164

RESEARCH PAPER

THERMO-MECHANICAL AND MICROSTRUCTURAL INVESTIGATIONS OF AA 6061/GNPS WELDED JOINTS DEVELOPED BY CONTINUOUS DRIVE FRICTION WELDING

Mohammed A. Tashkandi[1], *Mohammed Gamil*[2*]

[1]Department of Mechanical Engineering, College of Engineering, Northern Border University, Arar 90431, Saudi Arabia. ORCID: 0000-0002-1636-5122
[2]Department of Mechanical Engineering, Faculty of Engineering at Shoubra, Benha University, Cairo 11629, Egypt. ORCID: 0000-0002-8866-5829

*Corresponding author: mohammed.gamil@feng.bu.edu.eg, tel.: +201004635264, Faculty of Engineering at Shoubra / Benha University, 11629, Cairo, Egypt

Received: 06.08.2022
Accepted: 12.09.2022

ABSTRACT

The paper provides a novel technique for merging graphene nanoplatelets (GNPs) within aluminium matrix (AA 6061) by continuous drive friction welding (CDFW). The welding processes were done at 1400 rpm and 2000 rpm rotational speeds with two different frictional loads 2000 N and 2500 N for 5 sec and 7 sec welding times. The welded joints were subjected to tensile and hardness tests. The heating-cooling cycles through the welding process were monitored. The microstructure investigation was performed using optical and scanning electron microscopes (SEM). The effect of welding conditions on the ultimate tensile strength (UTS) results of AA 6061 and AA 6061/GNPs were completely studied in details. There is no big detectable variation in the mean hardness values due to the GNPs addition. The best welding conditions for achieving the highest mechanical properties were defined. The presence of GNPs in the welded joints results in lower heating at the welded joint at the same welding conditions. Finer grain structure and homogeneous distribution for the GNPs within the welding zone were observed.

Keywords: continuous drive friction welding; aluminum alloys; graphene nanoplatelets; metal matrix composites

INTRODUCTION

Friction welding is a general term for solid-state welding; it was first discovered by Thomas et al. [1]. The materials are joined in the solid state and viscous plasticity conditions without ever being melted or reached to a temperature close to the melting point. Friction welding has a variety of configurations and welding procedures. It can be classified into two main categories, which are rotational friction welding and friction stir welding. Rotational welding procedures include CDFW and inertia friction welding; they are usually used to weld tubes, rods of both similar and dissimilar materials. Friction stir welding and friction stir spot welding can be used to weld plates or replace mechanical joints such as rivets and bolts; both similar and dissimilar materials are utilized. Friction welding in general has many attractive advantages over conventional welding procedures such as absence of intermetallic layers in similar material welding, material integrity, cost, and environmental impact.

CDFW has been widely investigated in both similar and dissimilar material configurations. These configurations consist of welding similar material such as aluminium [2], Al 6063-T6 [3], AA 6060-T6 tubes [4], Al 2024 [5], Al 7075-T6 [6], Al 5052 [7] and AA6061 [8]; AA6061-T6 [9]. There have been numerous researches into welding dissimilar materials as well. The focus can be categorized into research related to steel/aluminium combinations in [10-17]. More recent studies investigated joining parts by CDFW in some innovative methods. The post-weld heat treatment of joints made CDFW for a composite compromised of AA6061, silicon carbide and graphite [18]. The best conditions for CDFW of another composite made of Al/SiCp utilizing Taguchi principles were investigated in an earlier study [19]. The joining of a solid bar of Al 6060 to a pipe made of Al-Si2CuNi alloy was also investigated [20]. Another composite material related CDFW study was concerned with joining Al/SiC to AISI 1030 steel; SiC particulates were used as a reinforcement material in AA 356 [21]. Another study investigated the characteristics of the joints by CDFW for Al/SiC composite [22]. Also, surface response plots and grey-based desirability were utilized to investigate joining Al/SiC/Al2O3 composites in CDFW [23]. HAZ microstructure and joint strength of metal matrix composites compromised of Al-Mg-Si and Al-SiC configurations were also investigated previously [24].

There have been some efforts into studying non-ferrous materials such as Mg alloys and related combinations [25,26], Ti alloys and related combination [27,28], Cu related investigations [29] and using CDFW to join ceramics and stainless steel [29,30]. Many research investigations into reviewing the state of CDFW have been published such as [31]; and more recently by [32-34]. Graphene is a sheet consisting of a single layer of carbon atoms. Graphene also when added to metallic alloys can increase the thermal expansion coefficient of the resulting metal matrix composite [35]. Adding graphene to metal alloys has been developed for materials such as AA6061-T6 used in friction stir welding [36], and AA5052 H32/GNPs [37]. But up to the time of writing this research manuscript, the authors did

not find any literature concerning the usage of GNPs in CDFW.
This study aims to investigate the effects of GNPs addition to AA 6061 by CDFW in terms of mechanical properties, thermal profiles, and surface morphology. A new test set up is designed and manufactured for applying the CDFW process by upgrading a conventional center lathe.

MATERIAL AND METHODS

Methodology

In the present study we designed and manufactured a CDFW machine by upgrading a conventional center lathe (see **Fig. 1**). The longitudinal force is applied by a pneumatic system and measured simultaneously by a load cell coupled with a digital load cell indicator. An electrical motor control circuit is designed to control the welding and upset times. A new low cost, simple, reliable and effective mechanical system is designed and fabricated to facilitate the work piece holding, force applying and braking the rotating chuck of the machine at the end of the desired welding time. **Fig. 2** presents different views for the clamping method of the piston holder with the carriage and bed. The shown design provides more flexibility for adjusting the axial distance between the chuck and the barrel.
Based on previous work done [8] where the same material was used in CDFW; tensile tests indicated failure outside the welded material within the parent material and such condition was achieved without performing any upsetting (forging stage). Therefore, the current study considered welding AA 6061 rods by CDFW and incorporating GNPs without any forging stage. The chemical composition of the aluminium rods (supplied from a local supplier) is tabulated in **Table 1**. Each welding rod was 65 mm long and 10 mm in diameter. Both welded sides were identical in dimensions.

Table 1 Chemical compositions of AA 6061 by wet%

Alloying element (wt%)								
Si	**Mg**	**Cu**	**Fe**	**Ti**	**Mn**	**Zn**	**Cr**	**Al**
0.75	0.9	0.5	0.5	0.15	0.05	0.03	0.03	97.09

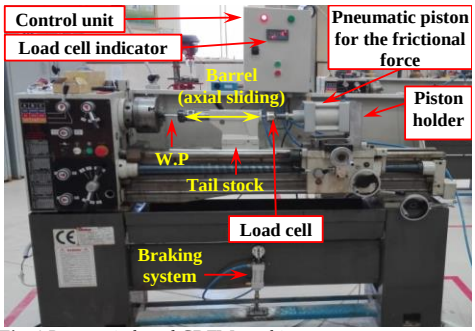

Fig. 1 Pneumatic-based CDFW machine.

GNPs in the form of graphene dispersion were supplied by Graphene Laboratories Inc. (760 Koehler Avenue - Suite 2 Ronkonkoma, NY 11779). The product is an ultra-high concentration dispersion of graphene with an average GNPs thickness of about 7 nm and 23 wt% total graphene content in N-Butyl acetate solvent. The rods were drilled in a way that the holes circumferential are touching the rod center (see **Fig. 3 (a)**). The hole has 3 mm diameter and 15 mm depth. After stirring the GNPs dispersion for 30 minutes as illustrated in the data sheet to provide complete homogeneous dispersion. The GNPs dispersion were injected into the holes. The hole was made sure to be fully filled with the GNPs dispersion. The samples were left for a few hours to let dry and then used in the CDFW. **Figure 3 (a, b)** show schematic and real images for the designed test setup with samples fixation within the rotating and fixed sides. The rotating side contains the AA 6061 with GNPs while the sample at the fixed side is AA 6061 only. During the welding process, the GNPs are moving out of the friction plane towards the periphery.

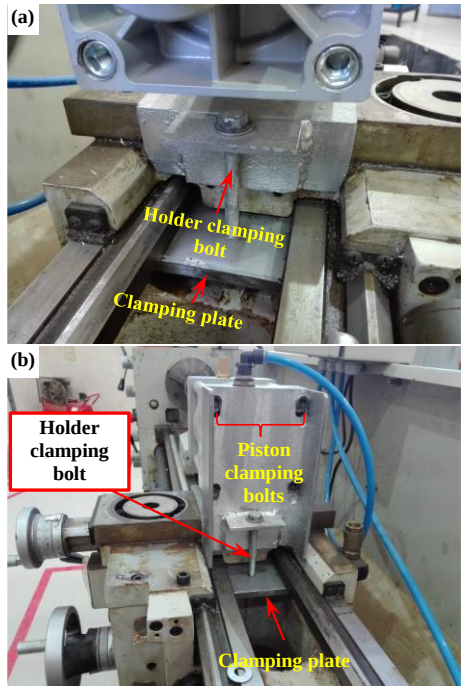

Fig. 2 Clamping method for the piston holder with the carriage and bed (a) Right hand side view (b) Left hand side view.

The welding procedure was performed next. The AA 6061 rods that were filled with GNPs were welded using our fabricated CDFW machine. The welding parameters for all samples are tabulated in **Table 2**. The reasoning behind choosing the levels of these parameters is attributed to previous work and trail-and-error runs. It was observed that for the material being used that rotational speeds ranging between 1400 and 2000 rpm, combined with frictional forces ranging between 2000 N to 2500 N; resulted in good welding with moderate flash formation. The friction time levels were chosen as 5 sec and 7 sec as previously observed, best tensile properties were obtained at 5 sec where failure almost always occurs outside the welded region and failure occurs mostly within the welded interface when the friction time exceeds 7 sec.

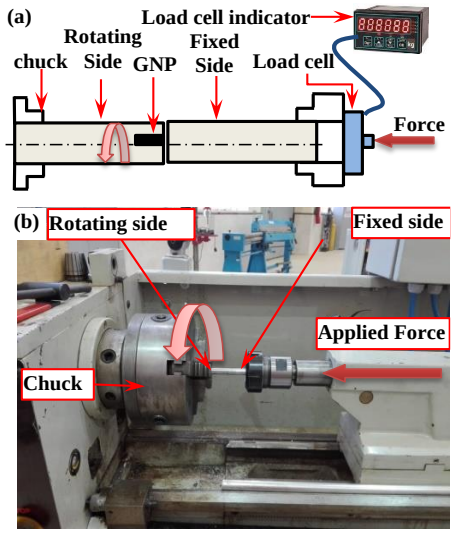

Fig. 3 CDFW process of AA 6061/GNPs (a) Schematics and (b) real images.

Table 2 CDFW parameters used for AA6061/GNPs

Experiment Number	Rotational Speed (RPM)	Frictional Force (N)	Friction Time (sec)
1	1400	2500	5
2			7
3		2000	5
4			7
5	2000	2500	5
6			7
7		2000	5
8			7

Material characterization

The as received GNPs were characterized by SEM and Raman Spectroscopy to ensure its quality. **Figure 4 (a)** shows an overlap flak structure with fewer wrinkles for the GNPs. In addition, **Fig. 4 (b)** illustrates that the flaks have few micrometers in dimensions without any visible defects. Raman spectroscopy analysis was conducted to ensure the quality of the as received GNPs dispersion. The three basic peaks D, G and 2D that distinguish GNPs were appeared at 1346.25, 1577.43 and 2712.08 respectively. The low intensity of the D peak reflects the high quality of the GNPs dispersion. Furthermore, the high ratio of ID/IG confirms the formation of small number of graphene layers (see **Fig. 5**) [37].

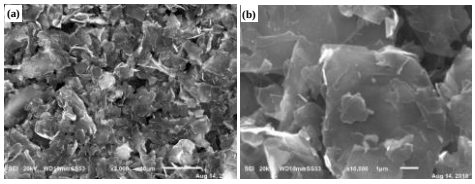

Fig. 4 SEM of the as received GNPs used for developing the AA 6061/ GNPs MMC by CDFW at magnifications (a) 2000 X and (b) 10000

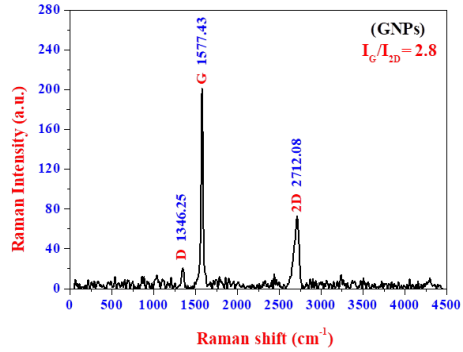

Fig. 5 Raman spectroscopy for the GNPs used for developing AA 6061/GNPs MMC.

Welded sample characterization

Characterization of the welded samples was achieved by tensile tests, micro-hardness, thermal analysis and microstructural investigation by optical microscopy (OM), SEM and energy dispersive x-ray (EDS). The thermal profile of the welding was video recorded utilizing a dual laser pointer. It has an operational range between -50 to 800 ºC, time accuracy is 0.5 sec, and a spatial accuracy of 1 mm. During the welding process, the temperature change in the laser pointer was video recorded, tabulated in excel and verified differences between samples with or without GNPs were observed. Tensile testing samples were prepared and tested according to ASTM:E8, and tensile tested with a rate of 0.5 mm/min via a computer controlled universal tensile testing machine (WDW-20). Vickers micro-hardness was performed to assess the changes in micro-hardness across all samples (Innovatest Europe BV NEMESIS 9104). The micro-hardness tests were performed with a load of 200 gram load and a dwell time of 10 sec. Finally, the samples used for microstructure were cut longitudinally with a fine cutter. Material preparations for microstructural examination included grinding, polishing, and etching were achieved as per standard practices for AA 6061. The microstructure of the samples was then observed using optical microscopy (Meiji MT 8530), and SEM capable of performing EDS (Zeiss Smart EDX).

RESULTS AND DISCUSSION

To iterate, CDFW utilizing AA 6061 rods infused with GNPs was performed. The effect of the process on the quality of the welding, mechanical properties and microstructure is to be investigated. The following sections discuss the tensile testing and hardness results, thermal welding profiles, and microstructure investigation.

Tensile results

Figures 6 and **7** show the tensile results for AA 6061 and AA 6061/GNPs at 1400 rpm and 2000 rpm respectively. **Figure 6 (a, b)** presents the tensile test results at 5 sec and 7 sec respectively; meanwhile the rotational speed and the frictional force are kept constant at 1400 rpm and 2500 N.
The AA 6061 sample had UTS of 300 MPa while the AA 6061/GNPs welded sample had an average of 252 MPa when the welding time was set to 5 sec (see **Fig. 6 (a)**). As the welding time was increased to 7 sec, the AA 6061 sample had UTS of 275 MPa while the AA 6061/GNPs welded samples had an UTS of 230 MPa on average (see **Fig. 6 (b)**).

Figure 6 (c, d) compares the tensile properties for the same welding conditions shown in **Fig. 6 (a, b)** with the exception of reducing the welding force to 2000 N. **Fig. 6 (c)** (5 sec) indicates that AA 6061 sample had an UTS of 253 MPa while the AA 6061/GNPs sample had an average UTS of 271 MPa. **Figure 6 (d)** (7s) indicates that the AA 6061 sample had an UTS of 238 MPa while the AA 6061/GNPs samples had an average of 256 MPa.

Figure 7 compares effect of the welding time on the tensile properties of the welded samples when the rotational speed was increased to 2000 rpm. **Figure 7 (a)** shows the tensile stress-strain curves for the samples welded at 2000 rpm, 2500 N, and 5 sec whereas **Fig. 7 (b)** shows the samples welded at 2000 rpm, 2500 N, and 7 sec. The AA 6061 welded samples at 5 sec had UTS of 299 MPa while the AA 6061/GNPs samples had average UTS of 262 MPa. On the other hand, the samples welded at a friction time of 7 sec had UTS of 276 MPa for the AA 6061 and average UTS of 164 MPa for the AA 6061/GNPs samples.

Lastly, the effect of the welding time on the tensile properties of the samples when the rotational speed and frictional force were 2000 rpm and 2000 N respectively is shown in **Fig. 7 (c, d)**. The stress strain curves shown on **Fig. 7 (c)** indicate that both the AA 6061 sample and the AA 6061/GNPs samples had UTS of 240 MPa. A slight difference among the two groups was observed in **Fig. 7 (d)**. Where the AA 6061 had UTS of 232 MPa and the AA 6061/GNPs samples had average UTS of 239 MPa.

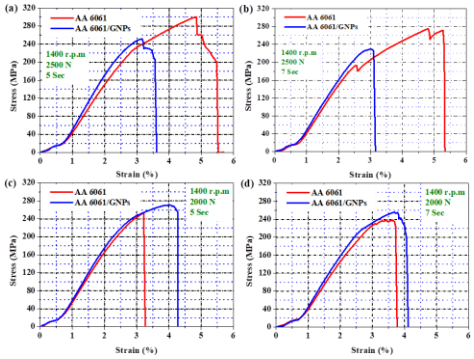

Fig. 6 Effect of GNPs addition to AA 6061 by CDFW on the tensile behavior at (a) 1400 rpm, 2500 N and 5 sec (b) 1400 rpm, 2500 N and 7 sec (c) 1400 rpm, 2000 N and 5 sec (d) 1400 rpm, 2000 N and 5 sec

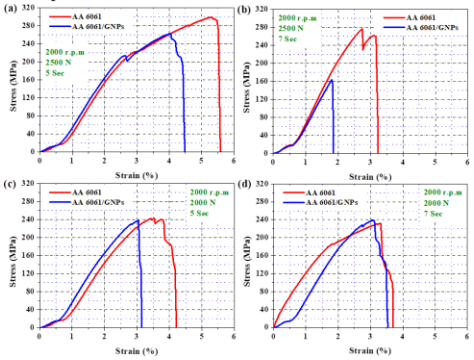

Fig. 7 Effect of GNPs addition to AA 6061 by CDFW on the tensile behaviour at (a) 2000 rpm, 2500 N and 5 sec (b) 2000 rpm, 2500 N and 7 sec (c) 2000 rpm, 2000 N and 5 sec (d) 2000 rpm, 2000 N and 7 sec

Figure 8 provides the UTS results of the welded samples AA 6061 and 6061/GNPs at different rotational speeds (1400 rpm, 2000 rpm), frictional forces (2500 N, 2000 N) and friction times (5 sec, 7 sec). It is noticed that the highest achievable UTS for AA 6061 and AA 6061/GNPs were 300 MPa and 271 MPa in experiments number 1 and 3, respectively. Consequently, it is recommended to perform the welding process according to the conditions of experiments 1 and 3 which are tabulated in **Table 2**.

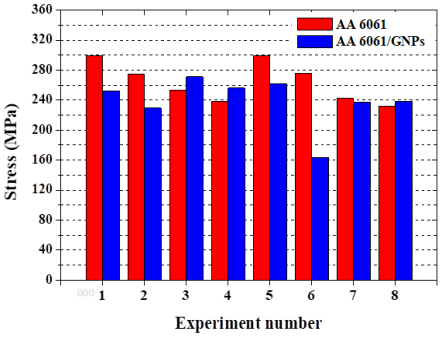

Fig. 8 Effect of rotational speed, frictional forces, and welding times on the UTS of the CDFW joints AA 6061 and AA 6061/GNPs

For AA 6061, there were no big detectable changes in the UTS between the experiments done at 1400 rpm (Experiments 1, 2, 3 and 4) and 2000 rpm (Experiments 5, 6, 7 and 8) (see **Fig. 9 (a)**). For AA 6061/GNPs, small variations in the UTS results were observed due to the change in the rotational speed in all test conditions except for test condition number 6. The big variation in the UTS of experiment number 6 is attributed to the presence of cracks; voids and GNPs agglomeration within the welding zone (see **Fig. 19**).

For AA 6061, decreasing the frictional force from 2500 N to 2000 N results in lowering the UTS for experiments 1, 2, 5 and 6 if they compared with experiments 3, 4, 7 and 8 respectively (see **Fig. 9 (c)**). On contrary, the UTS results of AA 6061/GNPs were increased when the frictional force decreased to 2000 N (see **Fig. 9 (d)**). The low friction force and low rotational speed give the chance for the GNPs to spread within the aluminium matrix to form MMC with higher strength. As a result, it is recommended to weld AA 6061/GNPs with the welding conditions of experiment 3 (lower speed 1400 rpm, lower friction force 2000 N and low friction time 5 sec) to achieve the best tensile results.

Generally, increasing the friction time from 5 sec (Experiment 1, 3, 5 and 7) to 7 sec (Experiments 2, 4, 6 and 8) reduced the UTS (see **Fig. 9 (e, f)**). So, it is recommended to perform the CDFW for AA 6061 and AA 6061/GNPs at 5 sec to achieve higher strength without time loss or more power consumption.

Hardness results

Figures 10 and **11** show the micro-hardness distribution for AA 6061 versus AA 6061/GNPs at the base metal (BM), heat affected zone (HAZ) and welding zone (WZ) at 1400 rpm and 2000 rpm. The effect of the friction time and force were studied as shown in **Fig. 10** and **Fig. 11**. It was noticed that the hardness distribution along the welding joints of AA 6061/GNPs is slightly lower than AA 6061 in most of the experiments. It seems that there is no big variation in the hardness values within the welding joints due to the time and

force variations. To provide a clear comparison between the welding conditions, the mean values of the harness distribution with their respect standard deviations were represented by the bar chart shown in **Fig. 12**. It was noticed that the values of mean micro-hardness are fluctuating with a narrow range (from 90 HV to 110 HV).

Fig. 12 shows the mean of the micro-hardness values of all samples. The highest micro-hardness value for the AA6061 samples was observed for experiment 2 with a very narrow error range. In contrast, the lowest value was observed for experiment 5 with a noticeable error range. On the other hand, the highest micro-hardness for the AA6061/GNPs samples was observed for experiments 1 and 7, with a smaller error range for experiment 1. In addition, the lowest micro-hardness for these samples was observed in experiment 8, as illustrated in **Fig. 12**. It seems that the micro-hardness values, in general, are higher when a lower rotating speed was used, which was represented by experiments 1 through 4 **(Fig. 12)**, which were conducted at 1400 rpm. Welding AA6061 rods while incorporating GNPs to obtain the best microhardness can be achieved by utilizing the process parameters from the first experiment.

Thermal Analysis

Figures 13 and **14** show the heating-cooling cycles for joining AA 6061 and AA 6061/GNPs at all the welding conditions tabulated in **Table 2**. Generally, the temperatures profile of all the welding conditions for AA 6061 and AA 6061/GNPs have similar trends, which rise to the peak and then drop. Lower heating and cooling rates for all the welded samples that contain GNPs have been observed. The lower heating and cooling rates in the presence of GNPs are attributed to the higher thermal conductivity of GNPs (~5300 W/m.K) [38]. The maximum detectable temperatures through the welding processes are in between 360 ºC and 506 ºC.

Figure 15 presents the maximum detectable temperatures result from the CDFW process for the AA 6061 and AA 6061/GNPs at all the welding conditions tabulated in **Table 2**. It was noticed that the increasing of welding time from 5 sec to 7 sec results in higher heat except in the welding conditions for experiment 6 that contains internal defects within its microstructure. The reduction of the heat generated in samples 3 and 4 than for samples 1 and 2 is attributed to the reduction in the applied force from 2500 N to 2000 N. Generally, the presence of graphene helps for increasing the heat dissipation due to its higher thermal conductivity. As a result, the maximum generated temperatures from the AA 6061/GNPs samples is lower than the AA 6061 samples except for samples 5 and 6 that have sever welding conditions which results in bad distribution for the GNPs within the welding zone.

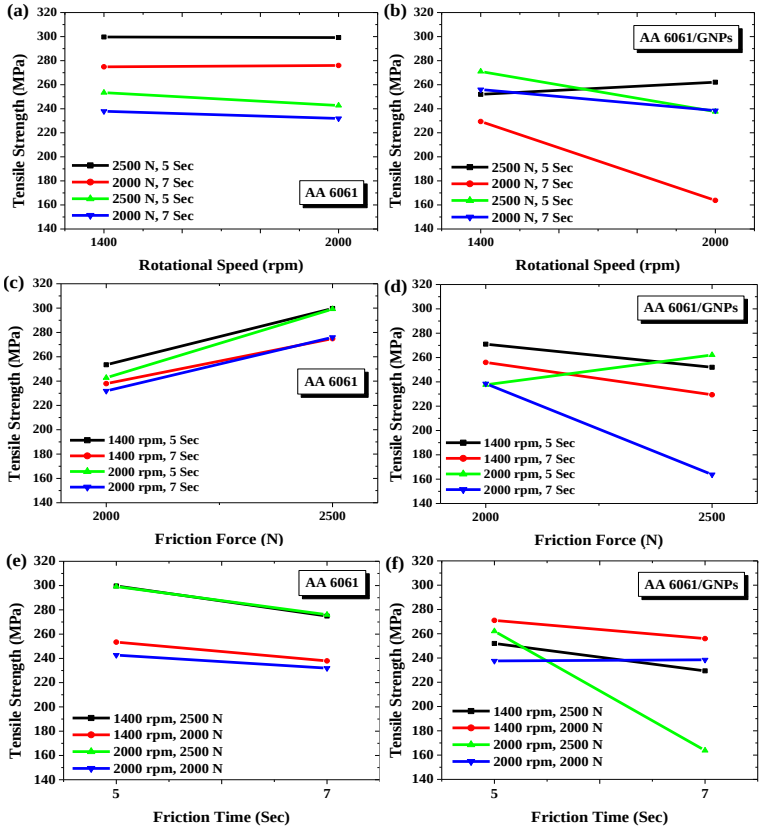

Fig. 9 Effect of welding conditions (rotational speed, friction time and friction force) on the UTS of AA 6061 (a, c, e) AA 6061/GNPs (b, d, f)

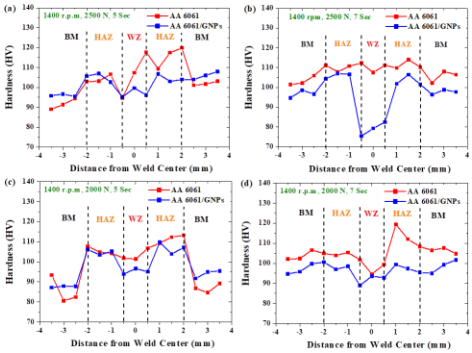

Fig. 10 Hardness distribution results of AA 6061 and AA 6061/GNPs at (a) 1400 rpm, 2500 N and 5 sec (b) 1400 rpm, 2500 N and 7 sec (c) 1400 rpm, 2000 N a;nd 5 sec (d) 1400 rpm, 2000 N and 5 sec.

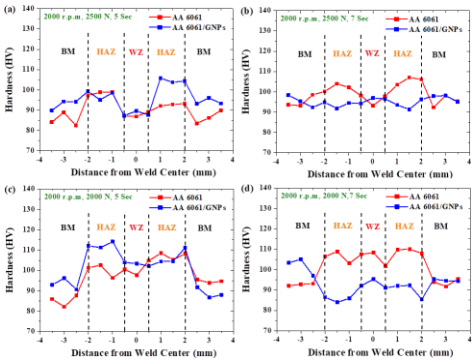

Fig. 11 microhardness distribution results of AA 6061 and AA 6061/GNPs at (a) 2000 rpm, 2500 N and 5 sec (b) 2000 rpm, 2500 N and 7 sec (c) 2000 rpm, 2000 N and 5 sec (d) 2000 rpm, 2000 N and 5 sec

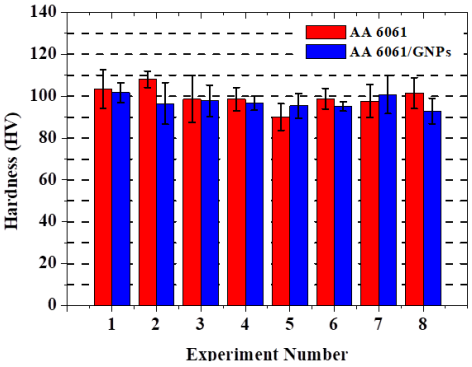

Fig. 12 Mean hardness values with standard deviation error bar for AA 6061 versus AA 6061/GNPs

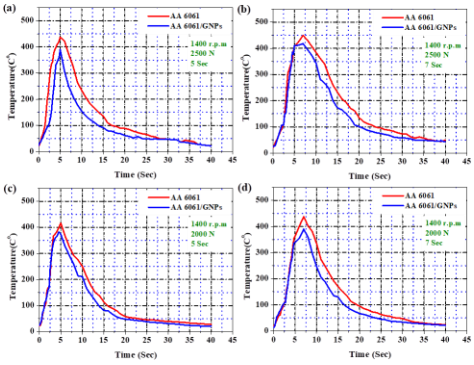

Fig. 13 Heating-cooling cycles for AA 6061 and AA 6061 at (a) 1400 rpm, 2500 N and 5 sec (b) 1400 rpm, 2500 N and 7 sec (c) 1400 rpm, 2000 N and 5 sec (d)1400 rpm, 2000 N and 7 sec

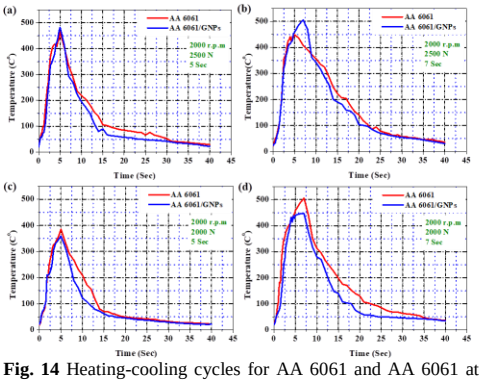

Fig. 14 Heating-cooling cycles for AA 6061 and AA 6061 at (a) 2000 rpm, 2500 N and 5 sec (b) 2000 rpm, 2500 N and 7 sec (c) 2000 rpm, 2000 N and 5 sec (d) 2000 rpm, 2000 N and 7 sec

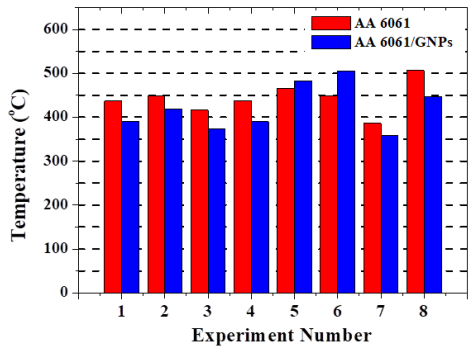

Fig. 15 Maximum temperature measured during CDFW for both AA6061 samples and samples with GNPs

Microstructure Investigation

Figure 16 shows the macrostructure for the welding joint of AA 6061 by CDFW. It shows the BM and HAZ within the rotating and fixed sides. In addition, the WZ in between the rotating and fixed sides is clearly shown. There is clear differ-

ence between the macrostructure between the different zones due to the heat generated from the CDFW process.

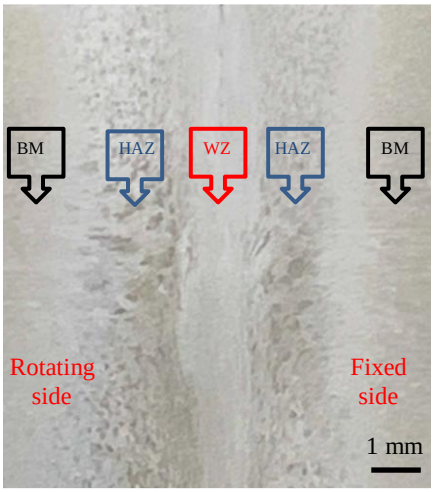

Fig. 16 Macro-structure of the welding joint for AA 6061

Figure 17 (a, b) presents the microstructure at two different magnifications for the welded joint of AA 6061 without GNPs at 1400 rpm, 2500 N and 5 sec. Meanwhile, **Fig. 17 (c, d)** shows the CDFW at the same conditions with the addition of GNPs to form the required MMC. It was seen that the CDFW results in finer grain structure near the welding zone due to the heat effect generated from the friction process. **Figure 17 (b)** depicts the normal microstructure of the AA 6061 with the impeded metallic inclusion referred in the **Fig. 17 (b,d)**. These metallic inclusions seem to be elliptical due to the rolling process. **Fig. 17 (c)** outlines the grain refining direction from the BM toward the stir WZ after the CDFW process for AA 6061 in the presents of GNPs at the same previous welding conditions. **Figure 17 (d)** illustrates higher magnification for the welding process presented in **Fig. 17 (c)**. The GNPs are well dispersed at the macroscopic scale through the base metal to form homogeneous MMC.

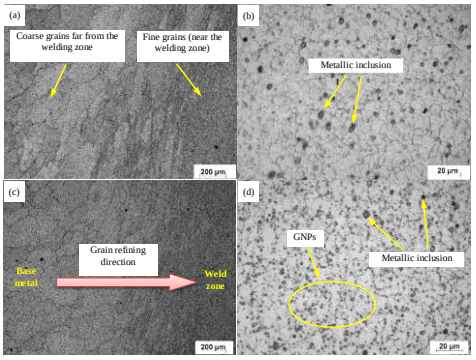

Fig. 17 Optical micrograph at low and high magnifications for joining Al 6061 by CDFW at 1400 rpm, 2500 N and 5 sec (a, b) without GNPs (c, d) with GNPs.

SEM was done in order to provide more microstructural investigation for the MMC formed at the welding zone. **Figure 18 (a, b)** represents SEM for the welding joint at 2000 rpm, 2500 N and 5 sec at two different magnifications. **Figure 18 (a)** shows excellent welding process without any cracks, voids and defects within the welding zone. In addition, homogeneous distribution for the GNPs within the welding zone was achieved. **Figure 18 (b)** illustrated the distribution of the GNPs within AA 6061 in the welding zone. Interestingly, GNPs are homogeneously distributed within the base metal and formed MMC with new mechanical and physical properties. Little agglomerations of GNPs within the MMC were noticed.

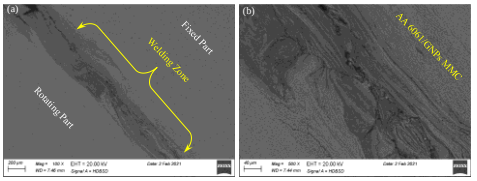

Fig. 18 SEM images for the welding joint at 2000 rpm, 2500 N and 5 sec at (a) low and (b) high magnifications

Figure 19 (a, b) presents SEM images for the WZ for experiment number 6 (2000 rpm, 2500 N and 7 sec) at low and high magnifications. The presence of micro-cracks, voids and GNPs agglomerations reflect the low measured UTS and microhardness values at this experiment.

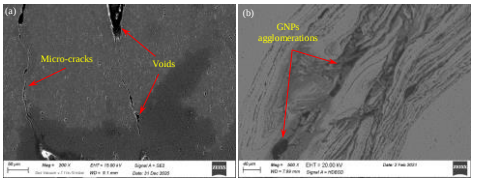

Fig. 19 SEM images for the welding joint at 2000 rpm, 2500 N and 7 sec.

Figure 20 shows the EDX point analysis for the MMC formed at the welding zone at at 1400 rpm, 2000 N and 5 sec in order to investigate the phases existed in the welding zone. The presence of carbon in the EDX refers to the presence of the GNPs within the MMC in an indication for homogeneous distribution to the GNPs within the matrix.

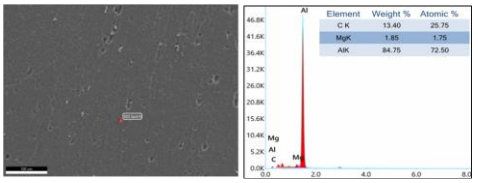

Fig. 20 EDX for the AA 6061/ GNPs MMC at 1400 rpm, 2000 N and 5 sec.

CONCLUSIONS

GNPs were merged into AA 6061 by a new investigated technique using CDFW to form new welded joints with new thermo-mechanical properties. The tensile strengths and microhardness were slightly decreased in the welded joints due to the GNPs addition. The heating-cooling cycles for the samples contain GNPs were occurred at lower temperatures. The microstructure investigations were referred to the homogeneous distribution for the GNPs within the welded joints except for experiment number 6. In addition, the EDX confirmed the

presence of GNPs within the aluminium matrix. Finally, the recommended welding parameters for AA 6061 and AA 6061/GNPs were defined.

Acknowledgments: Financial support from the Northern Border University, Grant No ENG-2018-3-9-F-7785 is gratefully acknowledged. The authors would also like to extend their thanks to Faculty of Engineering at Shoubra, Benha University for its support in implementing the project.

REFERENCES

1. W. Thomas, E. Nicholas, J. Needham, M. Murch, P. Temple-Smith, C. Dawes: Int Patent App PCT/GB92/02203, and GB Patent App 9125978.8, US patent, (5), 1995, 460-317.
2. B. S. Yilbas, A. Z. Sahin, A. Coban, B. A. Aleem: Journal of Materials Processing Technology, 54 (1-4), 1995, 76-81. https://doi.org/10.1016/0924-0136(95)01923-5.
3. B. Al Faizal, T. Amarnath, T. N. Roshan: International Journal of Engineering Trends and Technology (IJETT), 17 (5), 2014, 203-207.
http://dx.doi.org/10.14445/22315381/IJETT-V17P241.
4. G. D'Urso, M. Longo, C. Giardini: Microstructure and mechanical properties of Friction Stir Welded AA6060-T6 tubes, *Key Engineering Materials*, 554, 2013, 977-984.
http://dx.doi.org/10.4028/www.scientific.net/KEM.554-557.977.
5. P.-h. Geng, G.-l. Qin, Z. Jun, C.-a. Li: Transactions of Nonferrous Metals Society of China, 29 (12), 2019, 2483-2495. https://doi.org/10.1016/S1003-6326(19)65156-3.
6. M. Kimura, M. Choji, M. Kusaka, K. Seo, A. Fuji: Science and Technology of Welding and Joining, 10 (4), 2005, 406-412.
https://doi.org/10.1179/174329305X44125.
7. M. Kimura, M. Choji, M. Kusaka, K. Seo, A. Fuji: Science and Technology of Welding and Joining, 11 (2), 2006, 209-215.
https://doi.org/10.1179/174329306X89242.
8. M. A. Tashkandi, M. I. Mohamed: Engineering, Technology & Applied Science Research, 10 (3), 2020, 5596-5602. http://orcid.org/0000-0002-1636-5122.
9. X. Li, J. Li, F. Jin, J. Xiong, F. Zhang: Welding in the World, 62 (5), 2018, 923-930.
https://doi.org/10.1007/s40194-018-0601-y.
10. E. P. Alves, F. Piorino Neto, C. Y. An: Journal of Aerospace Technology and Management, 2 (3), 2010, 301-306.
https://doi.org/10.5028/jatm.2010.02037110.
11. A. Ambroziak, M. Korzeniowski, P. Kustroń, M. Winnicki, P. Sokołowski, E. Harapińska: Advances in Materials Science and Engineering, 2014, 2014, 1-15.
https://doi.org/10.1155/2014/981653.
12. O. D. Hincapié, J. A. Salazar, J. J. Restrepo, J. A. Graciano-Uribe, E. A. Torres: Engineering Journal, 24 (1), 2020, 129-144.
https://doi.org/10.4186/ej.2020.24.1.129.
13. N. Kumbhar et al.: Effect of Microstructure on Mechanical Properties of Friction- Welded Joints between Aluminum Alloys (6061, 5052) and 304 Stainless Steel, *Materials Processing and Texture*, edited by A.D. Rollett, Ceramic Transactions Series, 2008, 35-41.
http://dx.doi.org/10.1002/9780470444191.ch4.
14. S. D. Meshram, G. M. Reddy: Defence Technology, 11 (3), 2015, 292-298. https://doi.org/10.1016/j.dt.2015.05.007.
15. P. Sammaiah, A. Suresh, G. Tagore: Journal of Materials Science, 45 (20), 2010, 5512-5521.
https://doi.org/10.1007/s10853-010-4609-y.
16. M. G. Reddy, S. A. Rao, T. Mohandas: Science and Technology of Welding and Joining, 13 (7), 2008, 619-628.
https://doi.org/10.1179/174329308X319217.
17. M. Sahin: The International Journal of Advanced Manufacturing Technology, 41 (5-6), 2009, 487-497.
https://doi.org/10.1007/s00170-008-1492-7.
18. J. Senthilkumar, P. S. M. Kumar, V. Balasubramanian: Materials Research Express, 6 (12), 2020, 1261-1265.
https://doi.org/10.1088/2053-1591/ab6407.
19. A. Ramalingam, S. Muthuvel: International Journal of Manufacturing, Materials, and Mechanical Engineering, 7 (2), 2017, 19-37. https://doi.org/10.4018/IJMMME.2017040102.
20. M. Kimura, H. Sakaguchi, M. Kusaka, K. Kaizu, T. Takahashi: Journal of Materials Engineering and Performance, 24 (11), 2015, 4551-4560.
https://doi.org/10.1007/s11665-015-1735-3.
21. S. Celik, D. Gunes, Welding journal, 91 (8), 2012, 222S-228S.
22. R. Adalarasan, A. Shanmuga Sundaram: Journal of the Chinese Institute of Engineers, 39 (4), 2016, 484-492.
https://doi.org/10.1080/02533839.2015.1125792.
23. R. Adalarasan, M. Santhanakumar, A. Shanmuga sundaram: Journal of the Chinese Institute of Engineers, 40 (1), 2017, 55-65. https://doi.org/10.1080/02533839.2016.1271287.
24. O. Midling, Ø. Grong: Acta metallurgica et materialia 42 (5), 1994, 1611-1622.
https://doi.org/10.1016/0956-7151(94)90370-0.
25. İ. Çelikyürek, E. Önal, Anadolu University Journal of Science and Technology A - Applied Sciences and Engineering, 17 (3), 2016, 563-571.
https://doi.org/10.18038/btda.84126.
26. Z. Liang, G. Qin, H. Ma, F. Yang, Z. Ao: Science and Technology of Welding and Joining, 22 (5), 2017, 363-372.
https://doi.org/10.1080/13621718.2016.1248648.
27. M. Avinash, G. Chaitanya, D. K. Giri, S. Upadhya, B. Muralidhara: Microstructure and mechanical behaviuor of rotary friction welded titanium alloys, *Proceedings of world academy of science, engineering and technology*, Citeseer, 26, 2007, 426-428. https://doi.org/10.5281/zenodo.1078985.
28. P. Li, J. Li, M. Salman, L. Liang, J. Xiong, F. Zhang: Materials & Design (1980-2015), 56, 2014, 649-656.
https://doi.org/10.1016/j.matdes.2013.11.065.
29. Y. Wei, F. Sun, Advances in Materials Science and Engineering, 2018, 2018, 1-8.
https://doi.org/10.1155/2018/2809356.
30. P. Rombaut, W. De Waele, K. Faes: Friction welding of steel to ceramic, *Sustainable Construction and Design 2011 (SCAD)*, Ghent, Belgium, Ghent University, Laboratory Soete, 2 (3), 2011, 448-457.
31. M. Maalekian: Science and Technology of Welding and Joining, 12 (8), 2007, 738-759.
https://doi.org/10.1179/174329307X249333.
32. W. Li, A. Vairis, M. Preuss, T. Ma: International Materials Reviews, 61 (2), 2016, 71-100.
https://doi.org/10.1080/09506608.2015.1109214.
33. S. Kumar, C. Wu, G. Padhy, W. Ding: Journal of Manufacturing Processes, 26, 2017, 295-322.
https://doi.org/10.1016/j.jmapro.2017.02.027.
34. M.-K. Besharati-Givi, P. Asadi: *Advances in friction-stir welding and processing*, first ed., Elsevier, 2014.
35. V. Skákalová, A. B. Kaiser: *Graphene: properties, preparation, characterisation and devices*, first ed., Elsevier, 2014.
36. D. Jayabalakrishnan, M. Balasubramanian: Materials and Manufacturing Processes, 33 (3), 2018, 333-342.
https://doi.org/10.1080/10426914.2017.1339323.
37. M. Gamil, M. M. Ahmed: International journal of precision engineering and manufacturing, 21, 2020, 1539-1546.
https://doi.org/10.1007/s12541-020-00355-3.
38. A. A. Balandin, S. Ghosh, W. Bao, I. Calizo, D. Teweldebrhan, F. Miao, C. N. Lau: Nano letters, 8 (3), 2008, 902-907. https://doi.org/10.1021/nl0731872.